Science in China Series G: Physics, Mechanics & Astronomy

www.scichina.com
phys.scichina.com
www.springerlink.com

Basic function method

A new numerical method on unstructured grids

WU WangYi† & XIE WenJun

State Key Laboratory for Turbulence and Complex System, Department of Mechanics and Aerospace Engineering, College of Engineering, Peking University, Beijing 100871, China

A new numerical method—basic function method is proposed. This method can directly discrete differential operators on unstructured grids. By using the expansion of basic function to approach the exact function, the central and upwind schemes of derivative are constructed. By using the polynomial as basic function, applying the technique of flux splitting method and the combination of central and upwind schemes, the non-physical fluctuation near the shock wave is suppressed. The first-order basic function scheme of polynomial type for solving inviscid compressible flow numerically is constructed in this paper. Several numerical results of many typical examples for one-, two- and three-dimensional inviscid compressible steady flow illustrate that it is a new scheme with high accuracy and high resolution for shock wave. Especially, combining with the adaptive remeshing technique, the satisfactory results can be obtained by these schemes.

basic function scheme, new numerical method, unstructured grids

Nowadays numerical methods can be mainly classified into two categories, one is to discrete differential operator on structured grids such as the difference method, spectral method, the other is to discrete integral operator on unstructured grids, such as finite element method, finite volume method. The difference method has been widely used in the field of computational aerodynamics for a long time. And its analytic background has already been carefully studied in the past years. The difference method is highly-developed, simple and effective. However, it has its own limitations, such as it is difficult to deal with complex boundaries for the coordinate transform and joined-domain methods should be introduced, and it is also not easy to employ the adaptive remeshing technique in the difference method. Although the finite element method (FEM) has proved its superiority to the difference method in the aspects described above, FEM will cost much more CPU time and memory than difference method.

To enrich and develop the existing methods, we propose a new numerical method—basic function method. The method directly discretes differential operator on unstructured grids. We use the expansion of basic function to approach the exact function. A lot of orthogonal and complete family of functions can be used as basic function, for example, polynomial and trigonometric functions are in common use, and Legendre polynomial and Chebyshev polynomial also can be selected as basic functions to construct different kinds of basic function schemes. In this paper we use the polynomial of first order as basic function. To obtain the values of physic quantities at nodes, the governing equations of differential type are applied for basic function schemes. First, the central and upwind schemes of derivative are constructed at the nodes of unstructured grids. To verify the basic function method, we use it to solve the inviscid

Received April 7, 2009; accepted June 16, 2009
doi: 10.1007/s11433-009-0227-6
†Corresponding author (email: wuwy@pku.edu.cn)
Supported by the National Natural Science Foundation of China (Grant No.19889210)

Citation: Wu W Y, Xie W J. Basic function method. Sci China Ser G, 2009, 52(12): 2016-2026, doi: 10.1007/s11433-009-0227-6

compressible steady flow. Utilizing the technique of flux splitting and the combination of central and upwind schemes, the non-physical fluctuation near the shock wave is suppressed. In this paper we propose for the first time the common principle to construct the scheme with no spurious oscillations near the discontinuities on the basis of physical consideration and successfully construct the basic function scheme for solving inviscid compressible flow equations numerically. Several typical examples of one-, two-, and three-dimensional inviscid compressible flow are calculated and the accuracy and resolution of the shock waves are very satisfactory.

In the following only two-dimensional scheme is studied, the one- and three-dimensional scheme can be deduced in the same way.

1 The construction of the basic function

We use the expansion of basic function $\phi_i^{(n)}(x,y)$ to approach the exact function $f(x,y)$.

$$f^{(n)}(x,y)=\sum_{i=1}^{m} f(x_i,y_i)\phi_i^{(n)}(x,y). \tag{1}$$

In the formula above, $f^{(n)}(x,y)$ is the n-order approximation of exact function. $f(x_i,y_i)$ is the exact value on the node of element. Any orthogonal and complete family of functions may be used as basic function. The basic function in common use is polynomial and trigonometric function. When n is equal to different positive integer, different order approximating function can be obtained, and m is the number of basic functions in elements.

Only polynomial is used as basic function in this paper. And the basic function scheme of first-order-precision polynomial is studied here emphatically. Comparing with that of high-order-precision, the formula of basic function scheme of first-order-precision is simpler with much less node number, so the CPU time and memory needed are the least. And the accuracy and resolution of the shock waves can be improved through doing more remeshing.

In order to make the expression and derivation of formula more simple and convenient, area coordinate ξ_i is applied. We define

$$\xi_i = A_i / A. \quad (i=1,2,3),$$

where A is the area of the triangular element. The meaning of A_i have been shown in Figure 1. Obviously, the area coordinates satisfy $\xi_1+\xi_2+\xi_3=1$, so only two of them are independent. The relationship between ξ_i and cartesian coordinate comes as follows:

$$\xi_i = a_i + b_i x + c_i y, \tag{2}$$

where

$$\begin{aligned} a_i &= \frac{1}{D}(x_j y_k - x_k y_j),\\ b_i &= \frac{1}{D}(y_j - y_k),\\ c_i &= \frac{1}{D}(x_k - x_j) \end{aligned} \tag{3}$$

and

$$D=\begin{vmatrix} 1 & x_1 & y_1\\ 1 & x_2 & y_2\\ 1 & x_3 & y_3 \end{vmatrix} = 2A. \tag{4}$$

When n=1, eq. (1) can be rewritten as

$$f^{(1)}(x,y)=\sum_{i=1}^{3} f(x_i,y_i)\phi_i^{(1)}(x,y), \tag{5}$$

where $\phi_i^{(1)}(x,y)$ is the first order basic function of polynomial type. Its expression in area coordinates shows as follows (Figure 1):

$$\phi_i^{(1)}(x,y)=\xi_i, \quad (i=1,2,3). \tag{6}$$

The first order derivatives of $f^{(1)}$ are

$$\frac{\partial f^{(1)}}{\partial x}=b_i f_i, \quad \frac{\partial f^{(1)}}{\partial y}=c_i f_i, \tag{7}$$

where $f_i = f(x_i,y_i)$.

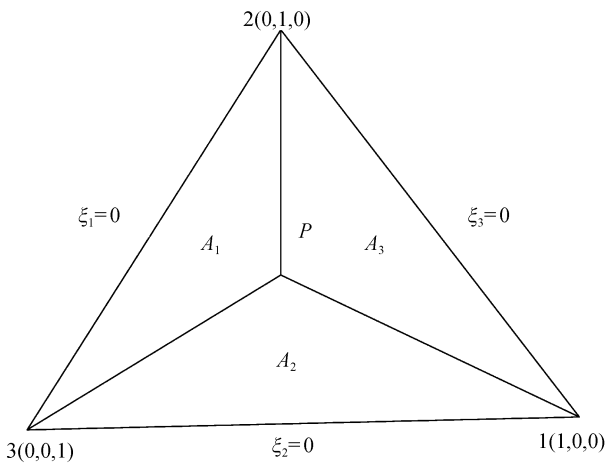

Figure 1 Area coordinate in a triangular element.

2 The central and upwind schemes of the derivative on unstructured grids

Now let us show how to construct the derivative of function at each node on unstructured grids. Due to the need of physical problem, the central scheme and the upwind scheme are introduced.

The first order central scheme (1C)

The central scheme means that the physical quantities on node are influenced by the message from all the directions. Assume there are N triangular elements around node n, and N different values of derivative $\left(\frac{\partial f^{(1)}}{\partial x}\right)_n^{e_i}$ $(i=1,2,...,N)$ on node n can be obtained, e_i stands for the ith triangular element around n. Utilize the weighted average method to obtain $\left(\frac{\partial f^{(1)}}{\partial x}\right)_n$ on node n. Because the less the area of the triangular element, the closer the value of $\left(\frac{\partial f^{(1)}}{\partial x}\right)_n$ to the exact value, so it is appropriate to choose $1/A_{e_i}$ as the weighted coefficient.

Now the central scheme of the first order derivative can be shown as follows:

$$\left[\frac{\partial f}{\partial x_j}\right]_n^{1C}=\frac{1}{\sum_{i=1}^{N}\frac{1}{A_{e_i}}}\sum_{i=1}^{N}\frac{1}{A_{e_i}}\left[\frac{\partial f^{(1)}}{\partial x_j}\right]_n^{e_i}\begin{pmatrix} j=1,2 \\ x_1=x, x_2=y\end{pmatrix}. \quad (8)$$

The first order upwind scheme (1U)

To obtain the upwind scheme of derivative on unstructured grids, the upwind area of triangular element is introduced. We can easily understand the meaning of upwind area in physics—only the upwind area has effect on the value of upwind derivative on that node.

We introduce upwind coefficient $\alpha_n^{e_i}$ to each node of every element. It relates to the element e_i and n, the order of the node in one element. Take the two-dimensional region shown in Figure 2, for example. there are four elements (i=1, 2, 3 and 4) in the region; the central node is always encoded as the first node of the element, no matter which element it belongs to; three nodes are encoded 1, 2 and 3 in a counterclockwise manner in one triangular; the flux is parallel to the x-axis. We use the perpendicular of x-axis through node n to split each triangular element around node n into upstream region and downstream region. We calculate the upwind coefficients in this problem and put them in Table 1.

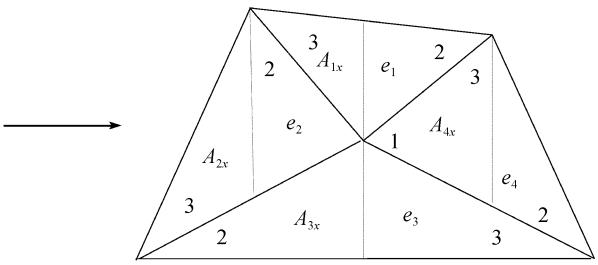

Figure 2 Upwind region of the unstructured grid.

Table 1 Upwind coefficients

Number of elements	Local number of nodes			$\alpha_1^{e_i}$		
e_1	1	2	3	$\frac{A_{1x}}{A_{e_1}}$	1	0
e_2	1	2	3	1	$\frac{A_{2x}}{A_{e_2}}$	0
e_3	1	2	3	$\frac{A_{3x}}{A_{e_3}}$	0	1
e_4	1	2	3	0	1	$\frac{A_{4x}}{A_{e_4}}$

The first order upwind scheme of the first order derivative is

$$\left[\frac{\partial f}{\partial x_j}\right]_n^{1U}=\frac{1}{\sum_{i=1}^{N}\frac{\alpha_n^{e_i}}{A_{e_i}}}\sum_{i=1}^{N}\frac{\alpha_n^{e_i}}{A_{e_i}}\left[\frac{\partial f^{(1)}}{\partial x_j}\right]_n^{e_i}\begin{pmatrix} j=1,2 \\ x_1=x, x_2=y\end{pmatrix}. \quad (9)$$

Apparently, if we assign all upwind coefficients $\alpha_1^{e_i}$ with value 1, the upwind scheme will be changed into the central scheme.

3 Basic function scheme for Euler's equation of inviscid compressible flow

We will base our discussion on compressible inviscid flow, which is governed by the Euler's equation:

$$\frac{\partial U}{\partial t}+\frac{\partial F_i}{\partial x_i}=0, \quad (10)$$

where

$$U=\left(\rho,\rho u_j,\rho\varepsilon\right)^{\mathrm{T}},$$

$$F_i=\left(\rho u_i,\rho u_i u_j+p\delta_{ij},u_i(\rho\varepsilon+p)\right)^{\mathrm{T}}.$$

ρ stands for the density of the gas, p for pressure; u_i is

the component of the vector of velocity under Cartesian coordinate system; ε is the specific energy of the gas and γ the ratio of specific heat (γ=1.4 in this article); δ_{ij} is the sign of Knonecker; superscript T represents the transposition of a vector, respectively.

3.1 Flux splitting technique

Equation (10) can be rewritten as

$$\frac{\partial U}{\partial t}+A\frac{\partial U}{\partial x_i}=0,\quad A=\frac{\partial F_i}{\partial U},\quad F_i=AU. \tag{11}$$

Matrix A can be written as

$$A=R^{-1}\Lambda R, \tag{12}$$

where Λ is the characteristic diagonal matrix. Its expression is

$$\Lambda=\mathrm{diag}\left(\lambda_1,\lambda_2,...,\lambda_m\right), \tag{13}$$

λ_l is the eigenvalue of matrix A. Define

$$\lambda_l=\lambda_l^+ +\lambda_l^-,\quad \lambda_l^{\pm}=\frac{\left(\lambda_l\pm|\lambda_l|\right)}{2}$$

and introduce

$$\Lambda^{\pm}=\mathrm{diag}\left(\lambda_1^{\pm},\lambda_2^{\pm},...,\lambda_m^{\pm}\right), \tag{14}$$

define

$$A^{\pm}=R^{-1}\Lambda^{\pm}R,\quad F_i^{\pm}=A^{\pm}U. \tag{15}$$

Equation (10) can be rewritten as

$$\frac{\partial U}{\partial t}+\frac{\partial F_i^+}{\partial x_i}+\frac{\partial F_i^-}{\partial x_i}=0. \tag{16}$$

3.2 Combination of central and upwind schemes

To avoid the spurious oscillations near the shock wave, proper scheme must be adopted in front of and behind the shock wave. The principle used in constructing non-oscillatory NND scheme of difference method[1] is right for one-dimensional model equation which cannot be utilized to deal with multi-dimensional problem in basic method. To overcome this difficulty, we propose for the first time the common principle to construct the scheme with no spurious oscillations near the discontinuities on the basis of physical consideration. First, let's consider the different physical characters before and after the shock wave. Every oblique shock wave can be seen as the combination of two normal shock waves in directions x and y. Supersonic flows always change into subsonic flows through normal shock waves, so there should be supersonic flow in front of the wave and subsonic flow behind the wave.

In consideration of the property that the perturbation downstream the supersonic flow can not propagate to the upstream then, to simulate the supersonic flow accurately, we must use upwind scheme in front of shock wave. On the contrary, for subsonic flow the perturbation downstream can propagate to the upstream, therefore we need to adopt central scheme behind the shock wave. After flux splitting, the appropriate schemes of the fluxes located on the two sides of shock wave are shown as Figure 3.

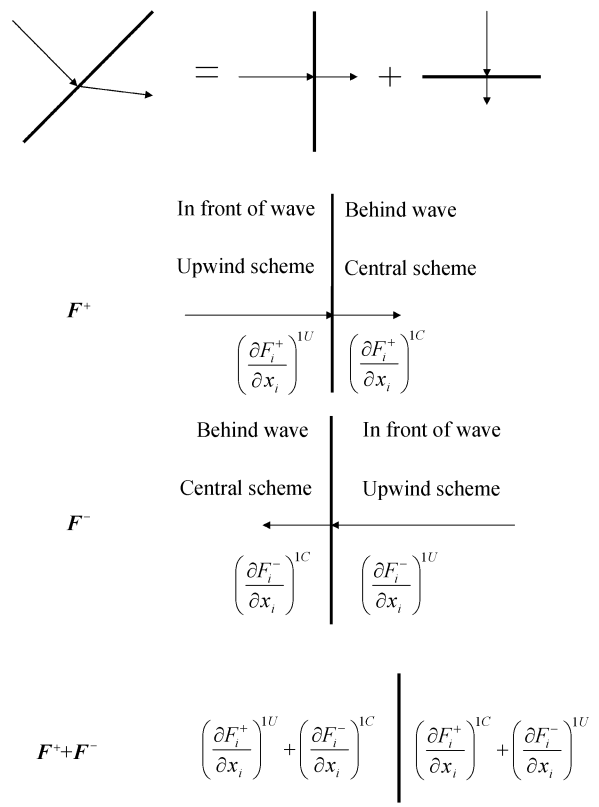

Figure 3 The basic function scheme of in front of and behind the shock wave.

3.3 Judgment of the location in the upstream of the discontinuity or in its downstream

After selecting the scheme, we should judge the position of a grid point—in the upstream of the discontinuity or in the downstream of it. Examining the distribution of the physical quantities on two sides of the shock wave, it is not difficult to find that the signs of the first derivative and the second derivative of the quantities are the same in front of the discontinuity and they are opposite behind it, and this is the principle to judge the location up or down the shock wave. For each node, the two one-side

derivatives of flux can be calculated. We write them down as δ^+F and δ^-F. Introduce

$$\delta^2F=\delta^+F-\delta^-F,\quad \delta F=\delta^+F+\delta^-F.$$

δ^2F and δF are something like second derivative and first derivative of the flux F respectively. The criteria for judging the location up or down the shock wave are:

$$\begin{cases}\delta^2F\cdot\delta F>0, & \text{if the point is in the upstream of the discontinuity,}\\ \delta^2F\cdot\delta F<0, & \text{if the point is in the downstream of the discontinuity.}\end{cases}$$

From the discussion of 3.2 and 3.3, the scheme between each side of the discontinuities should be chosen as Table 2[2].

Table 2 The scheme on each side of the discontinuities

	In upstream region of the discontinuity	In downstream region of the discontinuity
	signs of δ^2F and δF are the same	signs of δ^2F and δF are different
$a^+>0$	$\left[\frac{\partial F_i^+}{\partial x_i}\right]^{1U}$	$\left[\frac{\partial F_i^+}{\partial x_i}\right]^{1C}$
$a^-<0$	$\left[\frac{\partial F_i^-}{\partial x_i}\right]^{1C}$	$\left[\frac{\partial F_i^-}{\partial x_i}\right]^{1U}$
a^++a^-	$\left[\frac{\partial F_i^+}{\partial x_i}\right]^{1U}+\left[\frac{\partial F_i^-}{\partial x_i}\right]^{1C}$	$\left[\frac{\partial F_i^+}{\partial x_i}\right]^{1C}+\left[\frac{\partial F_i^-}{\partial x_i}\right]^{1U}$

3.4 Expression of the mixed scheme

Introduce

$$K=\frac{1}{2}\left|\text{sign}(\delta^2F)+\text{sign}(\delta F)\right|. \tag{17}$$

The first order explicit scheme combined by the basic function method and the method to suppress oscillation around the shock wave is shown as follows:

$$U^{n+1}=U^n-\Delta t\left\{K\left(\left[\frac{\partial F_i^+}{\partial x_i}\right]^{1U}+\left[\frac{\partial F_i^-}{\partial x_i}\right]^{1C}\right)+(1-K)\left(\left[\frac{\partial F_i^+}{\partial x_i}\right]^{1C}+\left[\frac{\partial F_i^-}{\partial x_i}\right]^{1U}\right)\right\}^n, \tag{18}$$

where

$$\left[\frac{\partial F_i^{\pm}}{\partial x_i}\right]_n^{1U}=\frac{1}{\sum_{j=1}^{N}\frac{\alpha_n^{e_j}}{A_{e_j}}}\sum_{j=1}^{N}\frac{\alpha_n^{e_j}}{A_{e_j}}\left[\frac{\partial F_i^{\pm(1)}}{\partial x_i}\right]_n^{e_j},$$

$$\left[\frac{\partial F_i^{\pm}}{\partial x_i}\right]_n^{1C}=\frac{1}{\sum_{j=1}^{N}\frac{1}{A_{e_j}}}\sum_{j=1}^{N}\frac{1}{A_{e_j}}\left[\frac{\partial F_i^{\pm(1)}}{\partial x_i}\right]_n^{e_j}.$$

Equation (18) is the first order explicit scheme we propose for the first time to deal with the compressible inviscid flow. In numerical simulation of compressible flows, boundary conditions are the non-reflection condition on exterior boundary and the tangential flow condition on body surface. The initial condition can be randomly assigned in the steady flow; but in the case of unsteady flow the initial condition must be raised specifically in correspondence to concrete problems.

4 Numerical examples

In order to test the effectiveness of the new basic function method, we apply it to 1 one-dimensional, 8 two-dimensional and 1 three-dimensional steady problems. We use mixing method of Delaunay triangulation and advance-front technique to generate grids[3,4], which can easily do mesh self-adaptive[5]. And to each problem, self-adaptive technique is used to improve the resolution near the discontinuity; and we deal with these steady problems using the time-dependent approach. In order to save space of this paper, the relative formulas for one-dimensional and three-dimensional problems will not written down, it is easy to derive them according to the procedure for the two-dimensional case if necessary.

Numerical example 1 is the one-dimensional shock wave tube. The initial parameters are $U(x,0)=U_L$ ($x<0$), $U(x,0)=U_R$ ($x>0$), $U_L=(1,0,2.5)^{\mathrm{T}}$, and $U_R=(0.125,0,0.25)^{\mathrm{T}}$. Figure 4 shows the pressure, density and velocity distribution we calculate in the shock wave tube, which agree very well with the exact solutions. Numerical example 2 is the steady compressible flow in two-dimensional passageway. There is a one-side shrinkage of 15° in the passageway. The Mach number of free stream is $M_\infty=2.0$. The numerical results of the self adaptive grids and isobars are shown in Figure 5. It can be easily seen that the resolution is high and all spurious oscillations are suppressed. Grids are highly condensed in the vicinity of the shock where the physics quantities change rapidly and the steep gradient near the shock is well captured. Numerical example 3 is the steady hypersonic flow around NACA 0012 airfoil. In

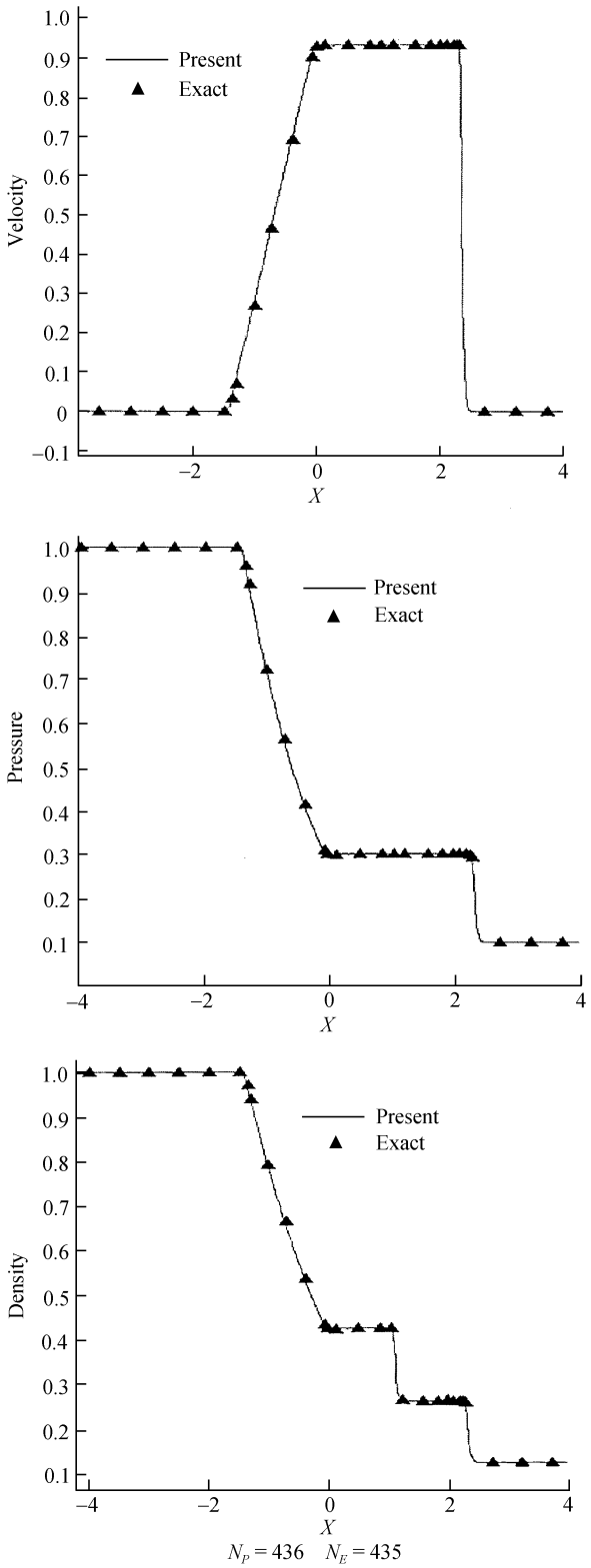

Figure 4 The pressure, density and velocity distribution calculated in the one-dimensional shock wave tube.

this problem, $M_\infty = 1.2$ and the angle of attack $\alpha = 7.0°$. Figure 6 depict the self-adaptive grids and isobars.

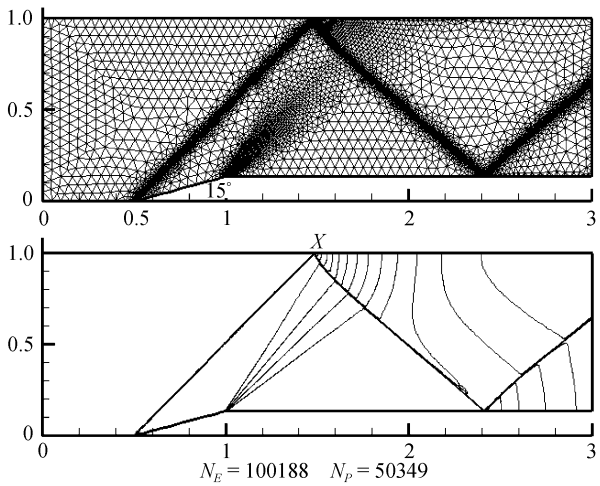

Figure 5 The self-adaptive grids and isobars of the steady compressible flow in two-dimensional passageway ($M_\infty = 2.0$).

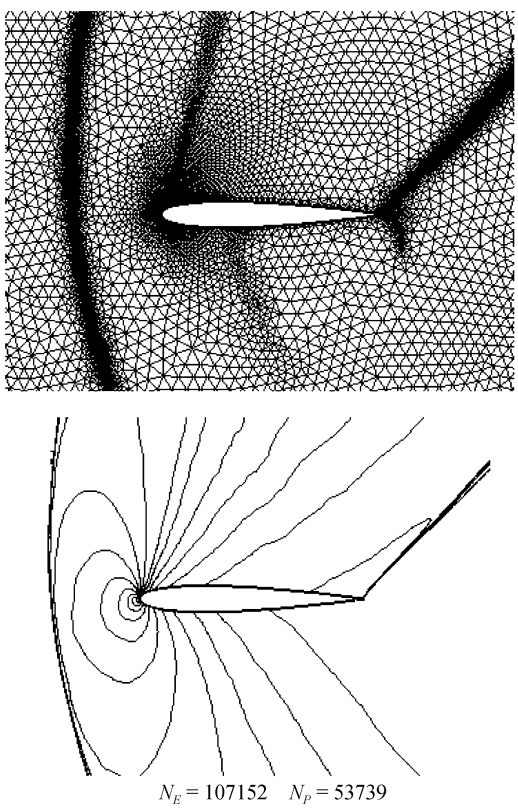

Figure 6 The self-adaptive grids and isobars of the steady hypersonic flow around NACA 0012 airfoil ($M_\infty = 1.2$, $\alpha = 7.0°$).

Both detached shock wave and the tail shock wave are captured with good accuracy and resolution. Figure 7 shows the distribution of pressure coefficient on the surface of the airfoil, which agree very well with the one given in ref. [6]. Numerical example 4 is the steady transonic flow around NACA 0012 airfoil. In this problem $M_\infty = 0.85$ and the angle of attack $\alpha = 1.0°$. The

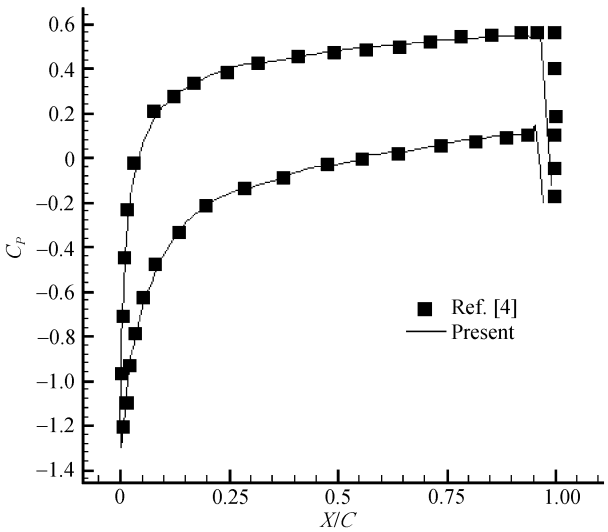

Figure 7 The distribution of pressure coefficient on the surface of NACA 0012 airfoil (M_∞= 1.2, α = 7.0°).

self-adaptive grids and isobars are shown in Figure 8. The shocks both on the upside and on the underside of the airfoil are captured clearly with good resolution. Figure 9 is the distribution of pressure coefficient on the surface of the airfoil, which is in good agreement with the result in refs. [6,7]. Numerical example 5 is a similar case of numerical example 4. The only difference between them is Mach number and the angle of attack. They are $M_\infty = 0.8,\ \alpha = 1.25°$. The self-adaptive grids and isobars are shown in Figure 10. There is only one shock wave on the upside of the airfoil. Figure 11 illustrates the distribution of pressure coefficients on the surface of the airfoil which agree with the result in refs. [6,7]. Numerical example 6 is the steady transonic flow around NACA 0012 airfoil problem. In this example, $M_\infty = 0.95$ and the angle of attack $\alpha = 0.0°$. We can see the self-adaptive grids and isobars in Figure 12. The two tail shock waves are captured clearly. Figure 13 shows the distribution of pressure coefficients on the surface of the airfoil, it agrees well with the result in ref. [6]. Numerical example 7 is the steady supersonic flow around a cylindrical body. In this problem, $M_\infty = 4.0$ and the angle of attack is zero. Figure 14 shows the self-adaptive grids and isobars; Figure 15 gives the pressure distribution on the wall. in comparison with the result in ref. [8], the agreement is very good. Numerical example 8 is the steady supersonic flow around a double ellipsoidal body. $M_\infty = 4.0$ and the angle of attack $\alpha = 0.0°$. The self-adaptive grids and isobars in Figure

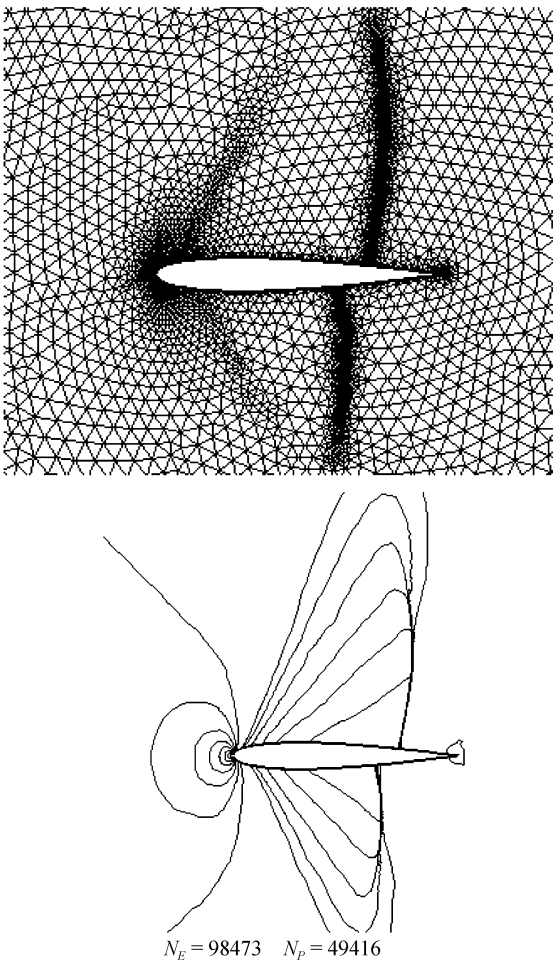

Figure 8 The self-adaptive grids and isobars of the steady transonic flow around NACA 0012 airfoil (M_∞= 0.85, α = 1.0°).

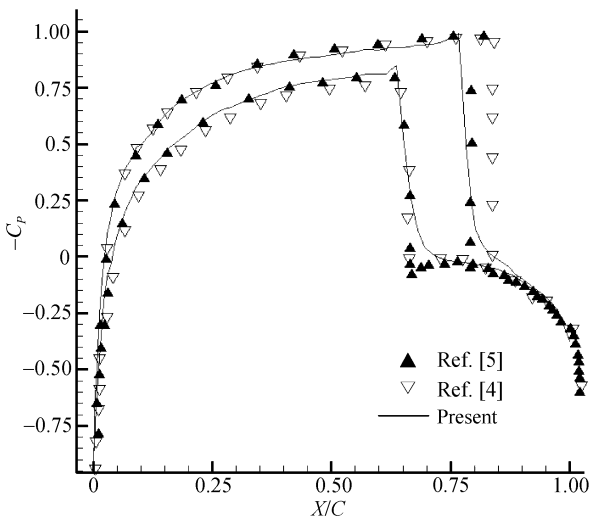

Figure 9 The distribution of pressure coefficient on the surface of NACA 0012 airfoil (M_∞= 0.85, α = 1.0°).

16 clearly show the intersection of the bow shock and the detached canopy shock and we can notice that the

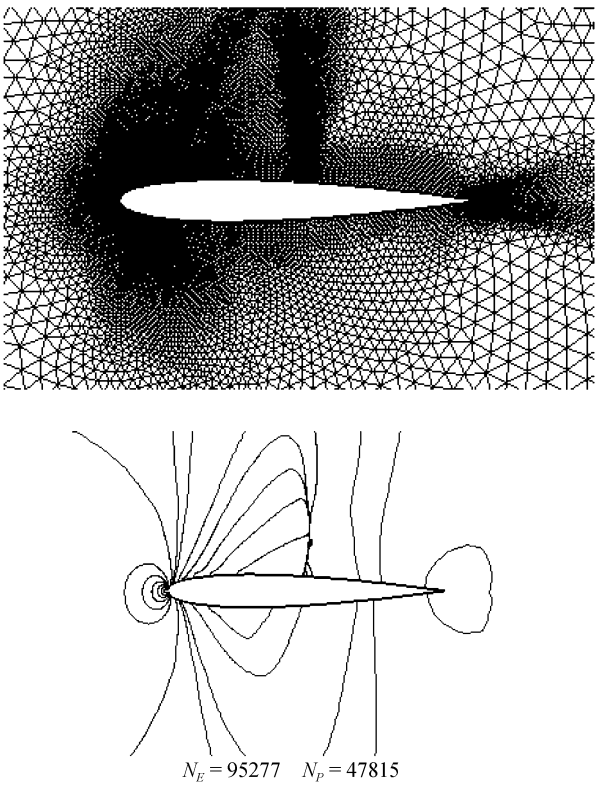

Figure 10 The self-adaptive grids and isobars of the steady transonic flow around NACA 0012 airfoil (M_∞= 0.8, α = 1.25°).

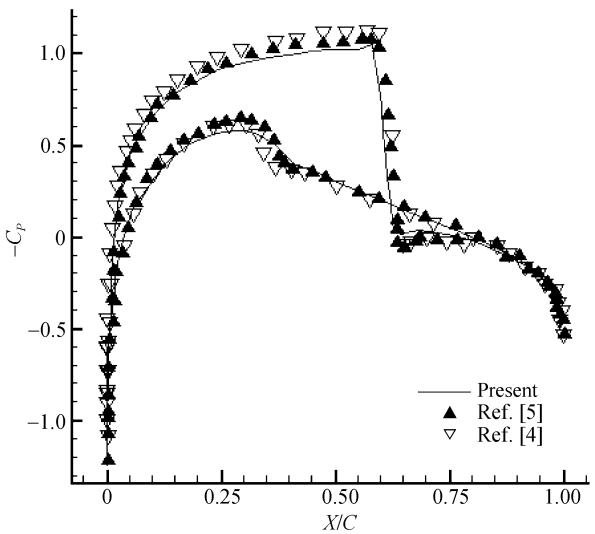

Figure 11 The distribution of pressure coefficient on the surface of NACA 0012 airfoil (M_∞= 0.8, α = 1.25°).

bow shock rises a little due to the influence of the canopy. Figure 17 displays pressure distribution on the wall. Numerical example 9 is the steady supersonic flow inside a staircase passageway. In this problem, $M_\infty = 3.0$ and the angle of attack $\alpha = 0.0°$. The height and width of the staircase separately are 0.2 and 2.5, and it is 0.5

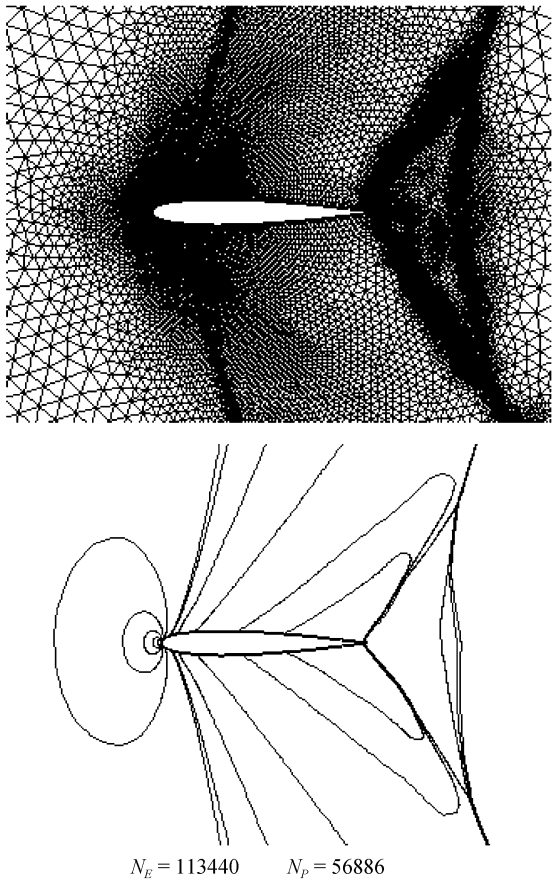

Figure 12 The self-adaptive grids and isobars of the steady transonic flow around NACA 0012 airfoil (M_∞= 0.95, α = 0.0°).

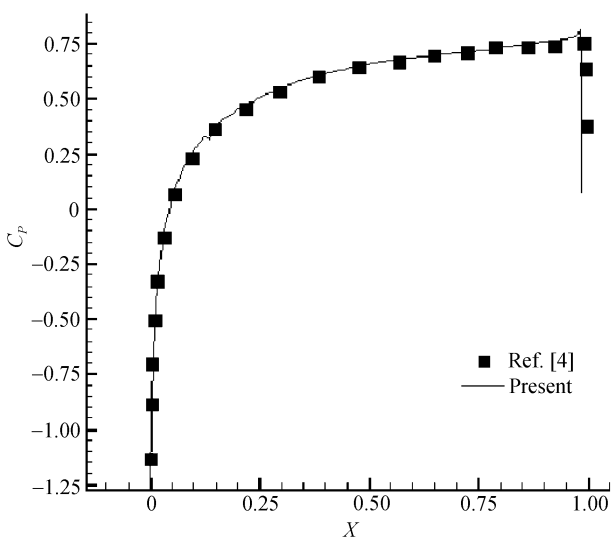

Figure 13 The distribution of pressure coefficient on the surface of NACA 0012 airfoil (M_∞= 0.95, α = 0.0°).

far from the entrance with height 1. The initial coefficients are u=1, v=0, p=0.079. The flow here is complex. It contains shocks, expansion waves and touch disconti-

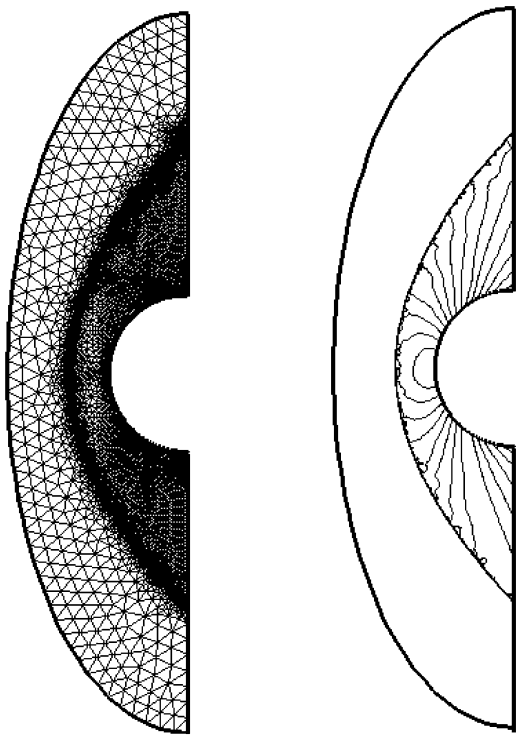

Figure 14 The self-adaptive grids and isobars of the steady supersonic flow around a cylindrical body (M_∞=4.0, α=0.0°).

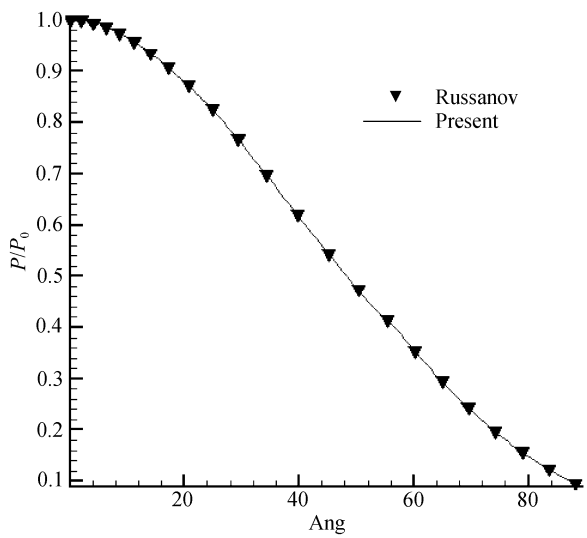

Figure 15 The pressure distribution on the wall of the steady supersonic flow around a cylindrical body (M_∞=4.0, α=0.0°).

nuities. Figure 18 is the self-adaptive grids and isobars. Numerical example 10 is the supersonic flow around a sphere. $M_\infty = 7.0$. It is an axisymmetric problem, but we regard it as a three-dimensional problem to test our three-dimensional scheme. The isobars in section *x*-*y* and the pressure distribution on the wall are given separately in Figures 19 and 20, and the pressure distribution

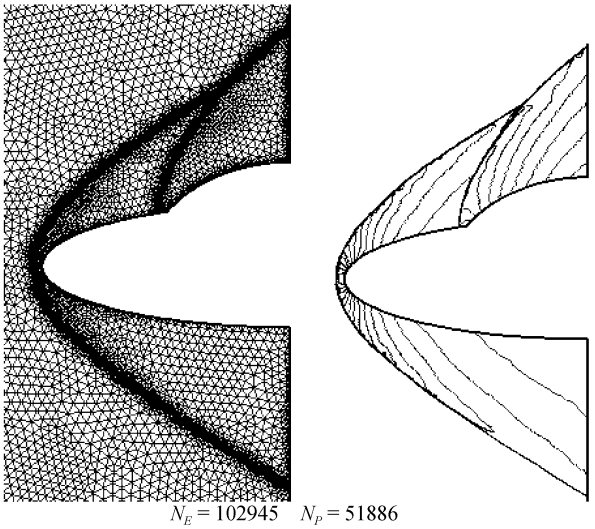

Figure 16 The self-adaptive grids and isobars of the steady supersonic flow around a double ellipsoidal body (M_∞=4.0, α=0.0°).

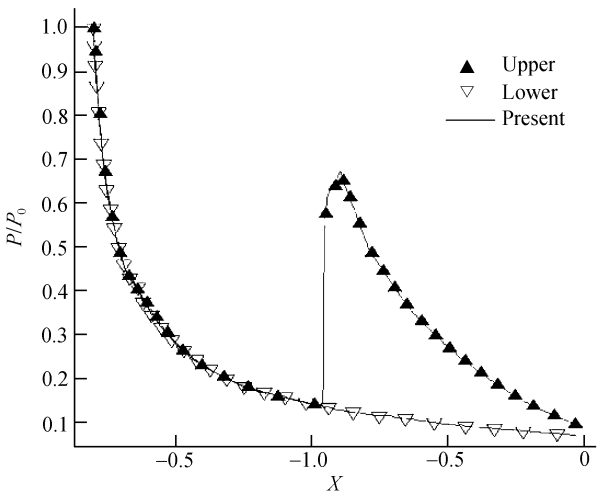

Figure 17 The pressure distribution on the wall of the steady supersonic flow around a double ellipsoidal body (M_∞=4.0, α=0.0°).

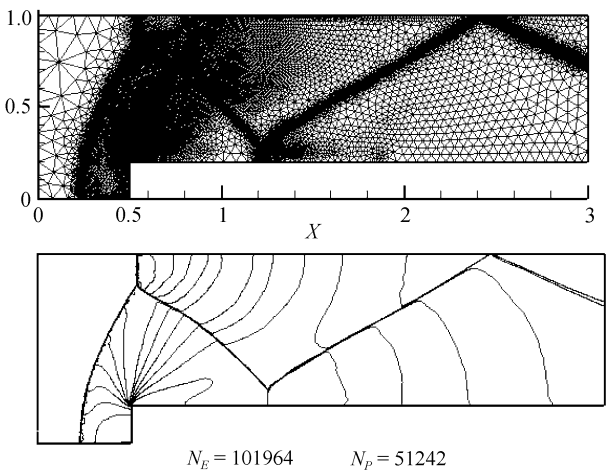

Figure 18 The self-adaptive grids and isobars of the steady supersonic flow inside a staircase passageway (M_∞=3.0, α=0.0°).

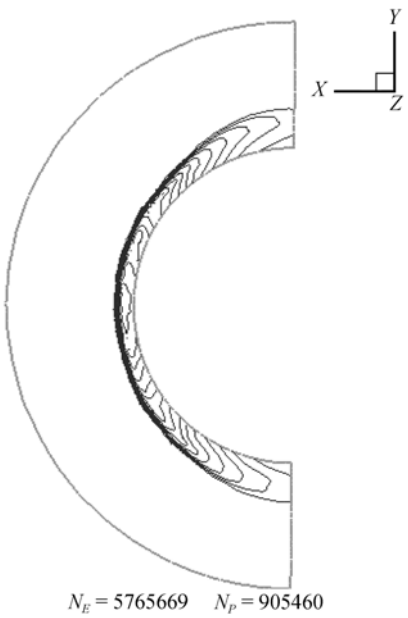

Figure 19 The isolines of pressure at the symmetrical section of y=0 of transonic flow around the three-dimensional sphere (M_∞= 7.0).

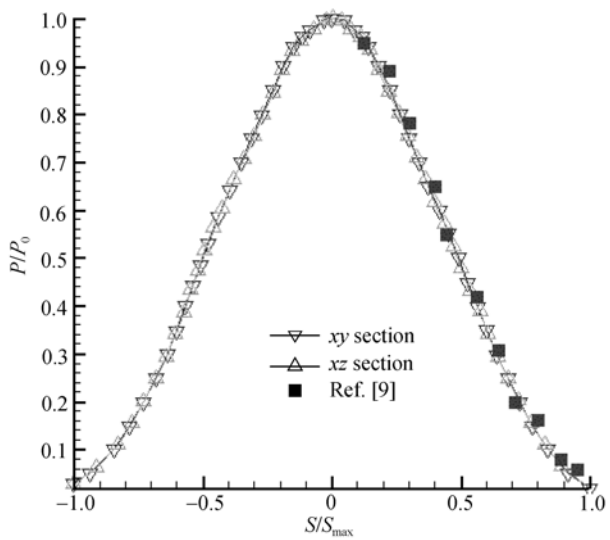

Figure 20 The pressure distribution at the symmetrical section of y=0 and z=0 on the wall of the steady transonic flow around the three-dimensional sphere (M_∞= 7.0).

is quite the same as ref. [9] (numerical example 10 is provided by Dr. Shen Fang).

5 Conclusions

1) In this paper we propose for the first time a new numerical method—basic function method, which can directly discrete differential operator. This method applies expansion of basic function to approach the exact function and construct successfully the central and upwind schemes of derivative on unstructured grids. Utilizing the technique of flux splitting and the combination of central and upwind schemes on the basis of physical consideration we obtain the first-order polynomial basic function scheme for inviscid compressible flows. Numerical solutions of several one-, two-, and three-dimensional typical problems show that combining with the adaptive remeshing technique, the schemes are non-oscillatory, of high resolution and the precision is satisfactory.

2) The basic function method preserves successfully some virtues of finite difference method and finite element method. First, because the basic function method is forwarded on the unstructured grids, which is the same as the finite element method it can easily handle complex boundary, keep the same scheme precision between the boundaries and the inside, and can apply self-adaptive remeshing technique to improve the accuracy of numerical results. Secondly, because the basic function method directly discrete differential operator, which is the same as the difference method, it can tremendously save CPU time and memory. Finally, another obvious speciality of basic function method is that the construction of these schemes are rather simple, normative and easy to develop universal numerical codes.

3) We focus our study on the basic function scheme of first-order-precision polynomial type. In comparison with the high-order-precision scheme, the formula of first-order-precision scheme is simpler with less node number, so the CPU time and memory needed are the least. And the accuracy and resolution of the shock waves can be improved through doing more remeshing. Practice shows that applying the first-order polynomial basic function scheme and combining with the adaptive remeshing technique, we not only tremendously save CPU time and memory but also obtain quite good results with high accuracy and high resolution.

4) According to the physical character, new common principle to construct the non-oscillatory scheme near the shock wave is proposed for the first time in this paper.

5) In this paper the basic function method has been studied in preliminary stage, next we should pay more attention to the theoretical basis of the method—accuracy analysis and stability analysis, besides, the further study of the basic function method should be also conducted for different type of fluid mechanic equations and different basic function.

1 Zhang H X. Non-oscillatory, containing no free parameters and dissipative differential scheme. Acta Aerodyn Sin, 1988, 6(2): 143－165
2 Wu W Y, Cai Q D. A new non-oscillatory, containing no free parameters and dissipative finite element schemes. Sci China Ser A-Math Phys Astron, 1998, 28(7): 633－643
3 Peraire J, Vahdati M, Morgan K, et al. Adaptive remeshing for compressible flow computations. J Comput Phys, 1987, 72: 449－466[DOI]
4 Xie W J. Research and application of the basic function method in the three-dimensional inviscid compressible flow and the generation of three-dimensional unstructured grid and the research of adaptive remeshing technique. Master Degree Dissertation. Beijing: Peking University, 2002. 1－48
5 Zeeuw D D, Powell K G. An adaptively refined cartesian mesh solver for the Euler equations. AIAA 91-1542 CP, 1991
6 Yee H C, Harten A. Implicit TVD scheme for hyperbolic conservation laws in curvilinear coordinates. AIAA J, 1987, 25(2): 266－274[DOI]
7 Hwang C J, Wu S J. Adaptive finite upwind approach on mixed quadrilateral-triangular meshes. AIAAJ, 1993, 31(1): 61－67[DOI]
8 Lyubimov A N, Rusanov V V. Gas flow past blunt bodies. NASA-TT-F715, 1973
9 Yamamoto Y. Numerical simulation of hypersonic viscous flow for the design of H-orbiting plane (HOPE). AIAA Paper, 90-0601

中国科学 G 辑: 物理学 力学 天文学 2009 年 第 39 卷 第 8 期: 1151 ~ 1160
www.scichina.com phys.scichina.com
《中国科学》杂志社
SCIENCE IN CHINA PRESS

一种新型的数值计算方法——基函数法

吴望一*, 谢文俊

北京大学工学院力学与空天技术系湍流与复杂系统国家重点实验室, 北京 100871

* E-mail: wuwy@pku.edu.cn

收稿日期: 2009-04-07; 接受日期: 2009-07-08

国家自然科学基金资助项目(批准号: 19889210)

摘要 我们提出一种新型的数值计算方法——基函数法. 此方法直接在非结构网格上离散微分算子. 采用基函数展开逼近真实函数, 构造出了导数的中心格式和迎风格式. 取多项式为基函数并采用通量分裂法及中心格式和迎风格式相结合的技术以消除激波附近的非物理波动, 我们构造出数值求解无黏可压缩流动一阶多项式的基函数格式. 通过一、二、三维多个无黏可压缩流动典型算例的数值计算表明本方法是一种高精度的, 对激波具有高分辨率的无波动新型数值计算方法, 与网格自适应技术相结合可得到十分满意的结果.

关键词
基函数法
新型数值计算方法
非结构网格

现有的数值方法可以分为两类: 一类是在结构网格上离散微分算子, 例如差分方法, 谱方法; 另一类是在非结构网格上离散积分算子, 例如有限元法和有限体积法. 它们各有特色, 也各有其优缺点. 有限差分法是计算流体力学领域中一种主要的数值计算方法, 它简单高效, 适应面广, 发展完善, 有众多优点. 但是不可否认, 它也有一些不尽人意之处. 处理复杂边界需要采用坐标变换或分区处理的办法, 比较麻烦. 其次, 也不易采用网格自适应技术有效地提高计算结果的精度. 边界上的格式精度往往比内点的格式精度要低. 有限元法是计算力学中另一类重要的数值计算方法. 由于有限元法采用非结构网格, 因此比较容易处理复杂边界, 也易于采用网格自适应技术提高计算精度. 而且有限元法有比较成熟的理论. 但是有限元法的计算时间及所需的内存都较有限差分法高出很多, 且逻辑复杂, 缺乏统一的构造格式的方法.

为了丰富和发展现有的计算方法, 本文提出一种新型的数值计算方法——基函数法. 此方法直接在非结构网格中离散微分算子, 生成网格后, 在网格单元上采用基函数展开逼近真实函数, 总体基函数逼近可以看作是由单元基函数组合而成的. 基函数可以取任意正交完备函数族, 常用的基函数是多项式和三角函数, 也可以取切贝谢夫多项式, 勒让德多项式等作为基函数, 从而构造出不同的基函数法. 本文取一阶多项式为基函数. 为了求出节点上的物理量, 基函数法采用微分形式的控制方程. 我们首先在非结构网格节点上构造出导数的中心格式和迎风格式. 为了验证基函数法, 本文运用此法数值求解无黏可压缩流动, 并采用通量分裂法及激波前后中心格式和迎风格式相结合的技术, 以消除激波附近的非物理波动, 为此, 本文根据物理考虑首次提出新的构造激波附近无波动格式的普适性准则, 由此构造出数值求解无黏可压缩流动的一阶多项式基函数格式.

引用格式: 吴望一, 谢文俊. 一种新型的数值计算方法——基函数法. 中国科学 G 辑, 2009, 39(8): 1151—1160
Wu W Y, Xie W J. Basic function method—A new numerical method on unstructured grids. Sci China Ser G, doi: 10.1007/s11433-009-0227-6

为了检验此方法, 我们对一、二、三维多个无黏可压缩流动的典型算例进行了数值计算, 均得到了十分满意的结果.

下面只考虑二维问题, 一维和三维问题可以类似地写出.

1 基函数的构造

采用基函数 $\phi_i^{(n)}(x,y)$ 展开逼近真实函数 $f(x,y)$,

$$f^{(n)}(x,y)=\sum_{i=1}^{m} f(x_i,y_i)\phi_i^{(n)}(x,y), \tag{1}$$

式中 $f^{(n)}(x,y)$ 是真实函数的 n 阶近似, $f(x_i,y_i)$ 是节点上的函数值. 基函数 $\phi_i^{(n)}(x,y)$ 可以取任意正交完备函数族, 最常用的基函数是多项式和三角函数. 当 n 取不同整数时, 可得不同阶次的逼近函数. m 是单元中基函数的个数.

本文只研究基函数是多项式的情形, 并重点研究一阶精度的多项式类型基函数格式. 这是因为和高阶精度相比, 一阶精度基函数格式的公式最简单, 涉及的单元节点个数最少, 因此所需的计算时间和内存也最少. 至于结果的精度和分辨率则完全可以通过自适应技术和加密网格的方法加以解决. 基于这样的认识, 我们着重研究一阶多项式基函数格式. 为了便于公式的推导和表达, 引入面积坐标 $\xi_i=A_i/A$ $(i=1,\ 2,\ 3)$, A 是三角形单元的面积, A_i 的意义见图 1. 因 $\xi_1+\xi_2+\xi_3=1$, 故三个面积坐标中, 只有两个是独立的. ξ_i 与直角坐标之间的关系为

$$\xi_i=a_i+b_i x+c_i y, \tag{2}$$

其中

$$\begin{aligned} a_i&=\frac{1}{D}\left(x_j y_k-x_k y_j\right),\\ b_i&=\frac{1}{D}\left(y_j-y_k\right),\\ c_i&=\frac{1}{D}\left(x_k-x_j\right), \end{aligned} \tag{3}$$

式中

$$D=\begin{vmatrix} 1 & x_1 & y_1\\ 1 & x_2 & y_2\\ 1 & x_3 & y_3 \end{vmatrix}=2A. \tag{4}$$

对于一阶多项式, (1)式可写为

$$f^{(1)}(x,y)=\sum_{i=1}^{3} f(x_i,y_i)\phi_i^{(1)}(x,y), \tag{5}$$

$\phi_i^{(1)}(x,y)$ 是一阶多项式类型的基函数, 它在面积坐标下的表达式为(图 1)

$$\phi_i^{(1)}(x,y)=\xi_i,\quad (i=1,\ 2,\ 3), \tag{6}$$

其一阶导数为

$$\frac{\partial f^{(1)}}{\partial x}=b_i f_i,\quad \frac{\partial f^{(1)}}{\partial y}=c_i f_i, \tag{7}$$

式中 $f_i=f(x_i,y_i)$.

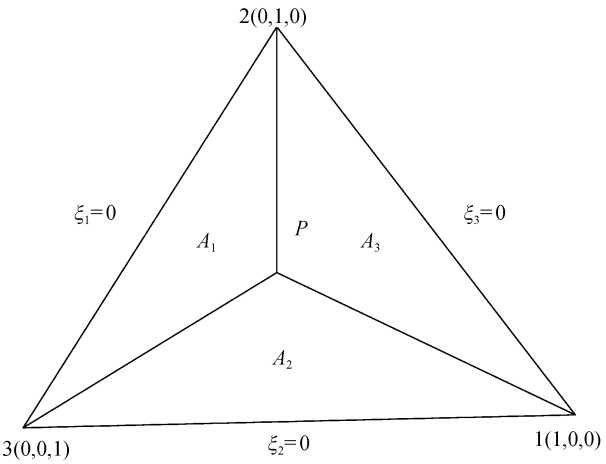

图 1 三角形单元的面积坐标示意图

2 非结构网格上导数的中心格式和迎风格式

下面我们来构造网格节点上函数的导数值. 根据物理问题的需要, 应区分中心格式和迎风格式两种情形.

一阶中心格式(1C): 中心格式是指一点的物理量受其周围各个方向的信息的影响. 设 n 点周围有 N 个三角元, 则根据(7)式在 n 点有 N 个不同的导数值 $\left(\frac{\partial f^{(1)}}{\partial x}\right)_n^{e_i}$ $(i=1,\ 2,\ \ldots,\ N)$. e_i 表示 n 周围第 i 个三角元. 下标 n 表示 n 点上的值. 我们采用加权平均法求 n 点上的函数值 $\left(\frac{\partial f^{(1)}}{\partial x}\right)_n$. 由于面积越小, $\left(\frac{\partial f^{(1)}}{\partial x}\right)_n$ 的值越接近精确值, 故权因子取 $1/A_{e_i}$ 是合适的.

于是一阶导数的中心格式是

$$\left[\frac{\partial f}{\partial x_j}\right]_n^{1C}=\frac{1}{\sum_{i=1}^{N}\frac{1}{A_{e_i}}}\sum_{i=1}^{N}\frac{1}{A_{e_i}}\left[\frac{\partial f^{(1)}}{\partial x_j}\right]_n^{e_i},\quad\begin{pmatrix}j=1,2\\x_1=x,x_2=y\end{pmatrix}. \tag{8}$$

一阶迎风格式(1U): 为了在非结构网格节点上构造导数的迎风格式, 我们提出三角元迎风面积的概念. 从物理上容易理解只有迎风面积这部分才对该点迎风导数值起作用.

对每个单元的每个节点引入迎风系数 $\alpha_n^{e_i}$, 它与单元 e_i 及局部节点编号 n 有关. 以图 2 所示的二维区域为例, 不失一般性, 假设有 4 个单元 $e_i(i=1,\ ...,\ 4)$. 中心点总体编号为 1, 4 个单元的局部节点按逆时针方向排序, 且总以中心点为第一点. 若 x 轴正向为迎风方向, 通过 n 点作 x 轴的垂线将 n 点周围每个三角元分成迎风面积和背风面积两部分. 此时我们有表 1 所示的迎风系数. 一阶导数的一阶迎风格式为

$$\left[\frac{\partial f}{\partial x_j}\right]_n^{1U}=\frac{1}{\sum_{i=1}^{N}\frac{\alpha_n^{e_i}}{A_{e_i}}}\sum_{i=1}^{N}\frac{\alpha_n^{e_i}}{A_{e_i}}\left[\frac{\partial f^{(1)}}{\partial x_j}\right]_n^{e_i}\begin{pmatrix}j=1,2\\x_1=x,x_2=y\end{pmatrix}, \tag{9}$$

容易看出, $\alpha_n^{e_i}$ 取为 1 时, 迎风格式转变为中心格式(8). 注意以上求导均是在一个三角单元中进行的. 上述构造中心格式和迎风格式的方法很容易推广到二阶及二阶以上, 三维及其他基函数的情形.

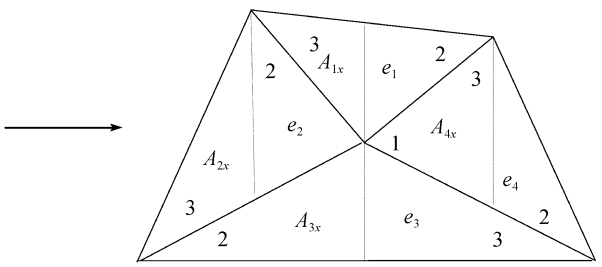

图 2 非结构网格迎风区域示意图

3 无黏可压缩流体 Euler 方程的基函数格式

考虑无黏可压缩流体的 Euler 方程:

$$\frac{\partial U}{\partial t}+\frac{\partial F_i}{\partial x_i}=0, \tag{10}$$

其中

$$\boldsymbol{U}=\left(\rho,\rho u_j,\rho\varepsilon\right)^{\mathrm{T}},$$

$$F_i=\left(\rho u_i,\rho u_i u_j+p\delta_{ij},u_i(\rho\varepsilon+p)\right)^{\mathrm{T}},$$

这里ρ是流体的密度, p 为压力, u_i 是直角坐标下的速度分量, ε表示流体的比能, 上标 T 表示向量的转置, γ为比热比, 取 $\gamma=1.4$, δ_{ij} 为 Knonecker 符号.

3.1 流通量分裂技术

(10)式可改写为

$$\frac{\partial \boldsymbol{U}}{\partial t}+\boldsymbol{A}\frac{\partial \boldsymbol{U}}{\partial x_i}=0,\quad \boldsymbol{A}=\frac{\partial F_i}{\partial \boldsymbol{U}},\quad F_i=\boldsymbol{A}\boldsymbol{U}, \tag{11}$$

将矩阵 $\boldsymbol{A}$ 写成

$$\boldsymbol{A}=\boldsymbol{R}^{-1}\boldsymbol{\Lambda}\boldsymbol{R}, \tag{12}$$

其中$\boldsymbol{\Lambda}$为特征对角线矩阵, 其表达式为

$$\boldsymbol{\Lambda}=\mathrm{diag}\left(\lambda_1,\lambda_2,...,\lambda_m\right), \tag{13}$$

λ_l 为 $\boldsymbol{A}$ 的特征值, 令

$$\lambda_l=\lambda_l^{+}+\lambda_l^{-},\quad \lambda_l^{\pm}=\frac{\left(\lambda_l\pm|\lambda_l|\right)}{2},$$

并引进

$$\boldsymbol{\Lambda}^{\pm}=\mathrm{diag}\left(\lambda_1^{\pm},\lambda_2^{\pm},...,\lambda_m^{\pm}\right), \tag{14}$$

令

$$\boldsymbol{A}^{\pm}=\boldsymbol{R}^{-1}\boldsymbol{\Lambda}^{\pm}\boldsymbol{R},\quad F_i^{\pm}=\boldsymbol{A}^{\pm}\boldsymbol{U}, \tag{15}$$

(10)式可改写为

$$\frac{\partial U}{\partial t}+\frac{\partial F_i^{+}}{\partial x_i}+\frac{\partial F_i^{-}}{\partial x_i}=0, \tag{16}$$

3.2 中心格式与迎风格式的结合

为了避免激波附近的非物理波动, 激波前后必须采用适当的格式. 在构造差分法的 NND 格式时, 为使二阶差分格式在间断附近无波动, 一阶模型方

表 1 迎风系数

单元编号	e_1			e_2			e_3			e_4		
局部节点号	1	2	3	1	2	3	1	2	3	1	2	3
$\alpha_1^{e_i}$	$\frac{A_{1x}}{A_{e_1}}$	1	0	1	$\frac{A_{2x}}{A_{e_2}}$	0	$\frac{A_{3x}}{A_{e_3}}$	0	1	0	1	$\frac{A_{4x}}{A_{e_4}}$

程的修正方程的色散项系数 μ_3 和耗散项系数 μ_4 应该满足以下两个准则[1]: (ⅰ) $\mu_4<0$, (ⅱ) 间断前 $\mu_3>0$, 间断后 $\mu_3<0$. 由于修正方程是一维的, 因此此准则不能用于处理多维问题的基函数方法中, 而且在基函数方法中也不存在修正方程. 为了解决此问题, 我们根据物理考虑首次提出新的构造无波动格式的普适准则.

首先, 让我们考虑一下激波前后的不同的物理特性. 任何一个斜激波在波前波后可以将其看作是在 x 和 y 两个方向分量的复合. 假设间断面与 x 和 y 方向均不重合, 由于斜激波的存在, 速度将减小, 很容易证明速度在波前 x, y 两个方向上的分量要分别大于波后 x, y 方向的分量. 即速度在 x, y 两个方向上都会发生间断, 因此可将斜激波看成是沿 x 方向和 y 方向的两个正激波的复合. 由于超音速气流在通过正激波后总会减速变为亚音速气流. 因此, 在分解后的两个方向的正激波的两侧, 总是波前是超音速流场, 波后为亚音速流场.

考虑到在超音速流场下游的扰动是无法传播到上游的, 为了能够正确地模拟超音速流场, 就必须符合该流场的物理特性. 因此, 在波前采用迎风格式是合适的. 相反, 在亚音速流场下游的扰动是可以传播到上游的. 因此, 在波后应该采用中心格式. 经过流通量分裂后, 各流通量在激波前后应采取的格式如图 3 所示.

3.3 间断前后的判断

选定格式后, 还必须能够在计算中判定网格点相对激波的位置. 考察激波前后物理量分布, 不难发现, 间断前, 物理量的一阶导数和二阶导数符号一致, 而间断后两者的符号则相反. 这就是间断前后的判断准则. 计算通量 F 在正负方向的两个单侧导数, 记为 $\delta^+\boldsymbol{F}$ 和 $\delta^-\boldsymbol{F}$, 引入:

$$\delta^2\boldsymbol{F}=\delta^+\boldsymbol{F}-\delta^-\boldsymbol{F},$$

$$\delta\boldsymbol{F}=\delta^+\boldsymbol{F}+\delta^-\boldsymbol{F},$$

$\delta^2\boldsymbol{F}$ 和 $\delta\boldsymbol{F}$ 分别与通量 $\boldsymbol{F}$ 的二阶导数和一阶导数相当. 由此间断前后的判断准则可表达为

$\delta^2\boldsymbol{F}\cdot\delta\boldsymbol{F}>0$, 则节点在间断上游;

$\delta^2\boldsymbol{F}\cdot\delta\boldsymbol{F}<0$, 则节点在间断下游.

根据 3.2 和本节的讨论, 间断两侧格式的选取如表 2 所示[2].

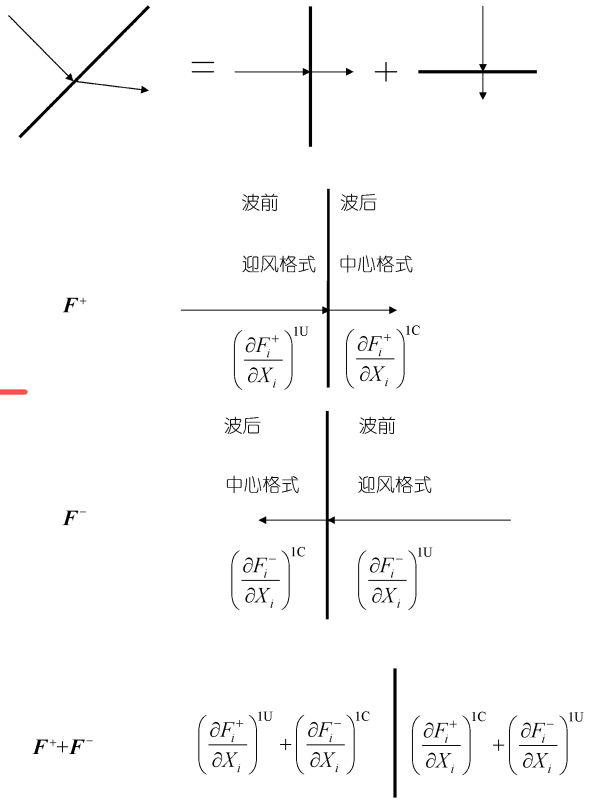

图 3 基函数法在激波前后的格式选取示意图

表 2 间断两侧格式的选取

	间断上游区	间断下游区
	δ^2F_i 与 δF_i 同号	δ^2F_i 与 δF_i 异号
$a^+>0$	$\left[\frac{\partial F_i^+}{\partial x_i}\right]^{1U}$	$\left[\frac{\partial F_i^+}{\partial x_i}\right]^{1C}$
$a^-<0$	$\left[\frac{\partial F_i^-}{\partial x_i}\right]^{1C}$	$\left[\frac{\partial F_i^-}{\partial x_i}\right]^{1U}$
a^++a^-	$\left[\frac{\partial F_i^+}{\partial x_i}\right]^{1U}+\left[\frac{\partial F_i^-}{\partial x_i}\right]^{1C}$	$\left[\frac{\partial F_i^+}{\partial x_i}\right]^{1C}+\left[\frac{\partial F_i^-}{\partial x_i}\right]^{1U}$

3.4 混合格式的表达

引进

$$K=\frac{1}{2}\left|\mathrm{sign}\left(\delta^2F_i\right)+\mathrm{sign}\left(\delta F_i\right)\right|, \tag{17}$$

采用基函数法及上述消除激波附近波动的方法所构成的一阶显式格式如下式所示:

$$U^{n+1}=U^{n}-\Delta t\left\{K\left(\left[\frac{\partial F_i^{+}}{\partial x_i}\right]^{1U}+\left[\frac{\partial F_i^{-}}{\partial x_i}\right]^{1C}\right)+(1-K)\left(\left[\frac{\partial F_i^{+}}{\partial x_i}\right]^{1C}+\left[\frac{\partial F_i^{-}}{\partial x_i}\right]^{1U}\right)\right\}^{n}, \quad (18)$$

式中

$$\left[\frac{\partial F_i^{\pm}}{\partial x_i}\right]_n^{1U}=\frac{1}{\sum_{j=1}^{N}\frac{\alpha_n^{e_j}}{A_{e_j}}}\sum_{j=1}^{N}\frac{\alpha_n^{e_j}}{A_{e_j}}\left[\frac{\partial F_i^{\pm(1)}}{\partial x_i}\right]_n^{e_j},$$

$$\left[\frac{\partial F_i^{\pm}}{\partial x_i}\right]_n^{1C}=\frac{1}{\sum_{j=1}^{N}\frac{1}{A_{e_j}}}\sum_{j=1}^{N}\frac{1}{A_{e_j}}\left[\frac{\partial F_i^{\pm(1)}}{\partial x_i}\right]_n^{e_j}.$$

(18)式就是我们首次提出的处理无黏可压缩流动的一阶精度的多项式基函数显式格式. 在数值求解可压缩流动时, 边界条件的取法是: 外部边界采用无反射边条件; 在壁面上采用法向速度为零的绕流条件. 初始条件是: 对于定常问题可任意取, 例如可取均匀来流条件; 对于不定常问题, 应视不同问题取不同的初始条件.

4 算例

为了验证基函数法, 选择了一个一维算例, 八个二维定常算例和一个三维定常算例. 我们采用前沿推进法或前沿推进法与Delaunay方法相结合的方法生成网格[3,4]. 该方法可方便地进行网格自适应[5]. 对每个算例都进行了初网格计算并采用网格自适应技术以提高对间断的分辨能力. 在计算中采用时间相关法处理定常问题. 为了节省篇幅, 一维和三维的有关公式不再写出, 它们很容易仿照二维的做法推出.

算例 1 考虑一维激波管, 初始参数为 $U(x,0)=U_L$ ($x<0$ 时), $U(x,0)=U_R$ ($x>0$ 时), $U_L=(1,\ 0,\ 2.5)^{\mathrm{T}}$, $U_R=(0.125,0,0.25)^{\mathrm{T}}$. 图 4 给出了计算得到的激波管内压力, 密度和速度的分布, 与准确解符合得很好. 算例 2 是二维通道内可压缩流体的定常流动, 单侧收缩 15°, 来流 $M_\infty=2.0$. 图 5 是计算得到的自适应网

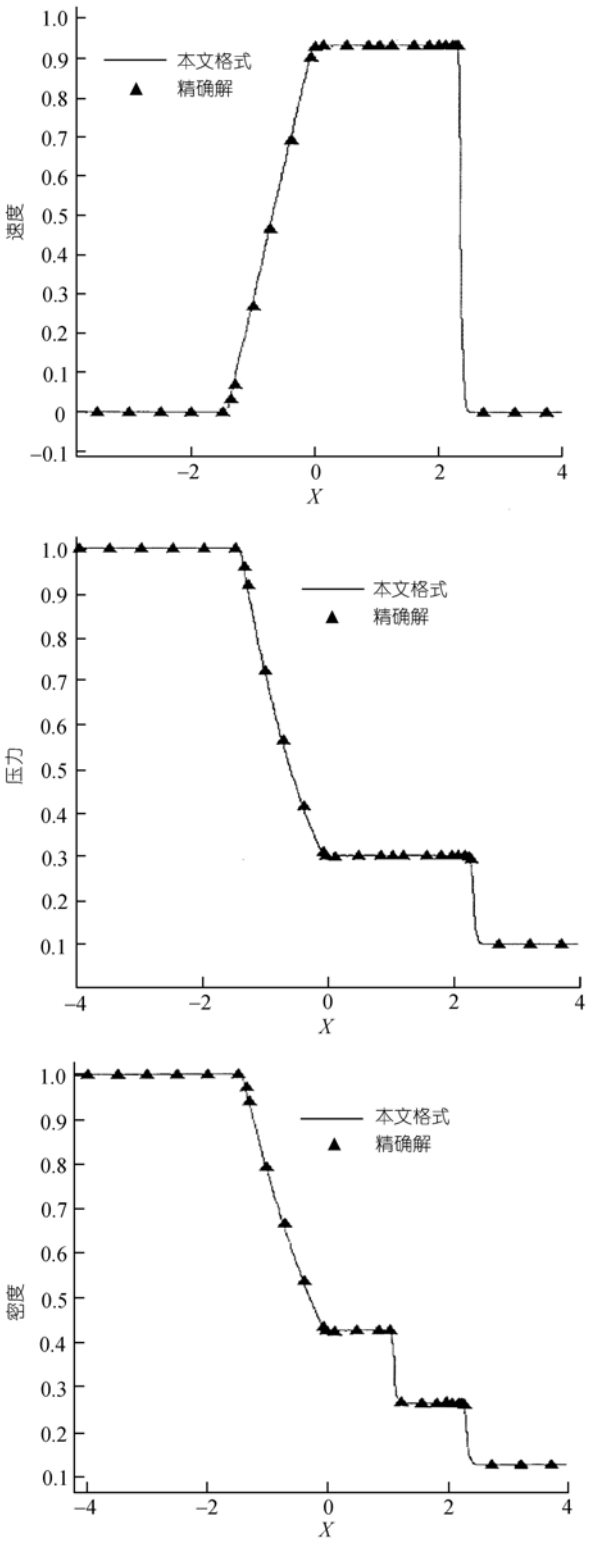

图 4 一维激波管自适应后算出的速度、压力和密度分布

NP = 436, *NE* = 435

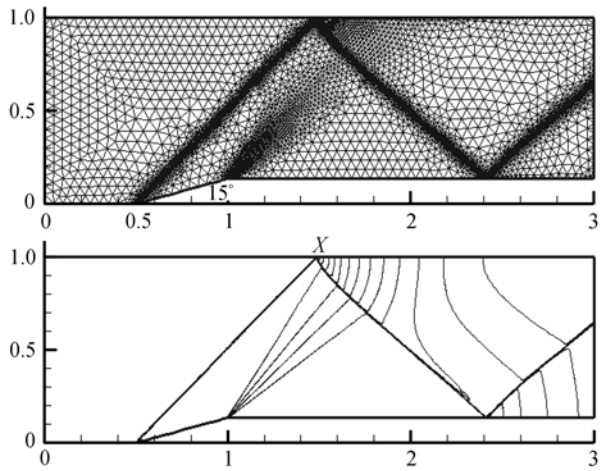

图 5　二维通道流动自适应网格及等压线分布(M_∞=2.0)

NE = 100188, *NP* = 50349

格及等压线分布图. 可以看出, 整个流动分辨率高, 无数值波动. 自适应使得网格在物理量变化剧烈的激波附近加密, 效果十分显著. 算例 3 是 NACA 0012 翼型定常超音速绕流, M_∞ = 1.2, 攻角α = 7.0°. 图 6 是自适应网格和等压线分布图. 可以看出, 计算结果对脱体激波和尾部激波的捕捉和分辨率都比较好. 图 7 是翼型表面压力系数的分布曲线, 与文献[6]中的结果符合得很好. 算例 4 是 NACA 0012 翼型定常跨音速绕流, M_∞ = 0.85, 攻角α = 1.0°. 图 8 是自适应网格和等压线分布图. 计算可清晰地捕捉到翼面上下激波, 并具有较好分辨率. 图 9 是翼型表面压力系数分布曲线, 与文献[6,7]符合得较好. 算例 5 和算例 4 是同一情形, 只是 M_∞ 和α 不同, 分别是 M_∞ = 0.8, α = 1.25°. 图 10 是自适应网格和等压线分布图. 此时只有翼型上表面有激波. 图 11 是翼型表面压力系数分布曲线图, 与文献[6,7]的结果基本符合. 算例 6 是 NACA 0012 翼型定常跨音速绕流, M_∞ = 0.95, 攻角α = 0°. 图 12 是自适应网格和等压线分布图, 能清晰地捕捉到尾部上下两条激波. 图 13 是翼型剖面压力系数分布图, 与文献[6]符合得很好. 算例 7 是圆柱的定常超音速绕流, 来流 M_∞ = 4.0, 攻角α = 0°. 图 14 是自适应网格及其等压线分布. 图 15 是壁面压力分布. 与文献[8]比较, 两者相当吻合. 算例 8 是双椭圆外形的超音速定常绕流, 来流 M_∞ = 4.0, 攻角α = 0°. 图 16 是自适应网格和等压线分布图. 可以看出, 座

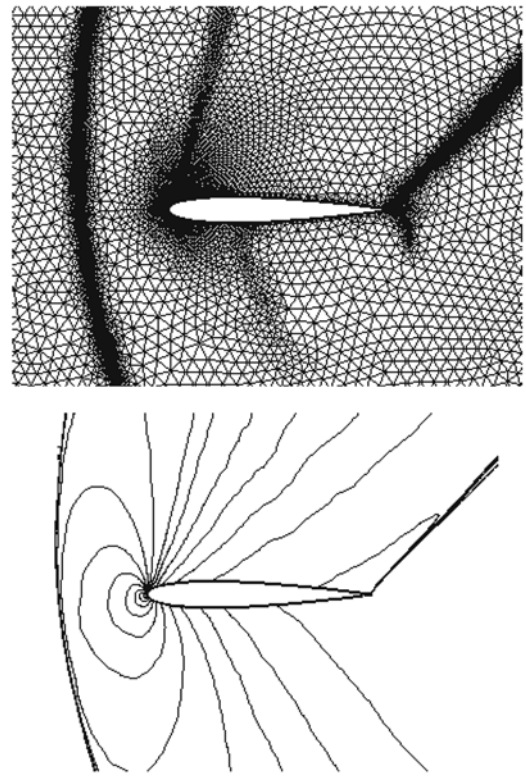

图 6　NACA 0012 翼型自适应网格和等压线分布图(M_∞= 1.2, α = 7.0°)

NE = 107152, *NP* = 53739

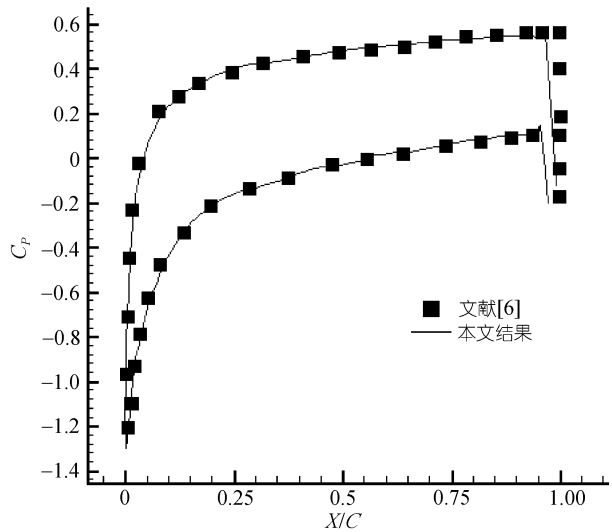

图 7　NACA 0012 翼型表面压力系数分布图(M_∞=1.2, α=7.0°)

舱前的激波是脱体的, 并且与头激波相交, 使得头激波在座舱上方略向上抬起. 图 17 是翼面压力分布图. 算例 9 是前台阶超音速绕流, 来流 M_∞ = 3.0, 攻角

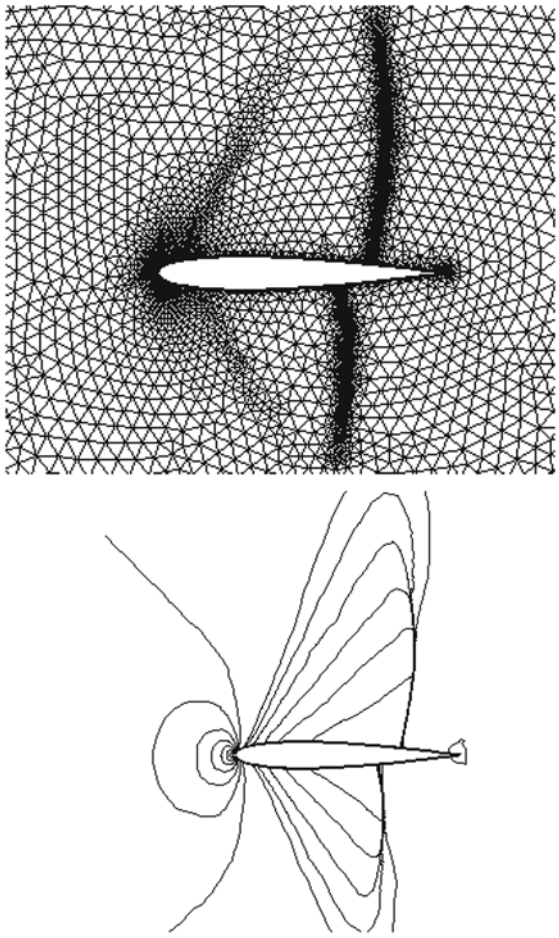

图 8 NACA 0012 翼型定常跨音速绕流自适应网格和等压线分布图(M_∞=0.85, α=1.0°)

NE = 98473, *NP* = 49416

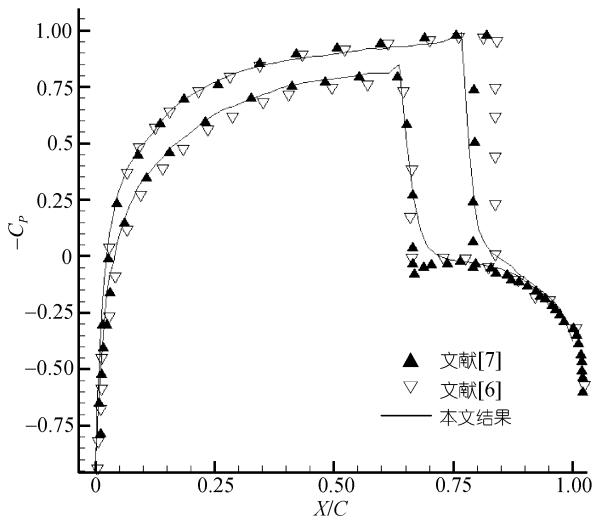

图 9 NACA 0012 翼型表面压力系数分布图(M_∞=0.85, α=1.0°)

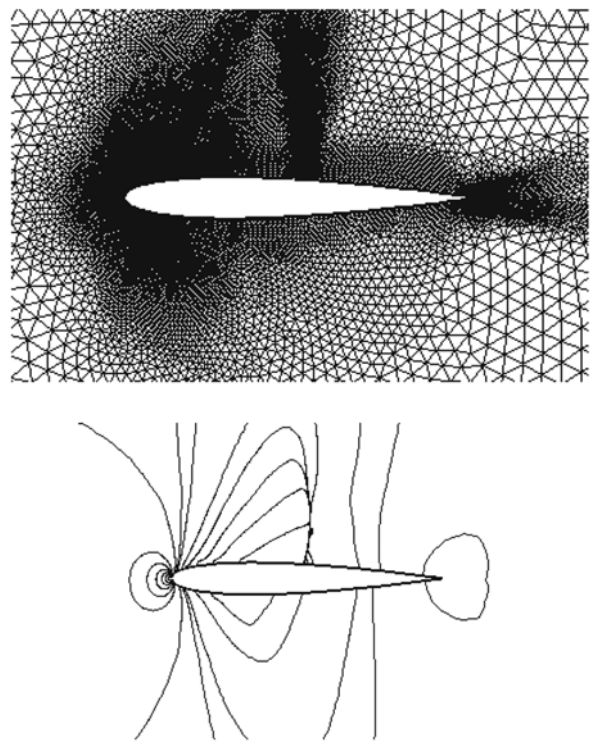

图 10 NACA 0012 翼型定常跨音速绕流自适应网格和等压线分布图(M_∞=0.8, α=1.25°)

NE = 95277, *NP* = 47815

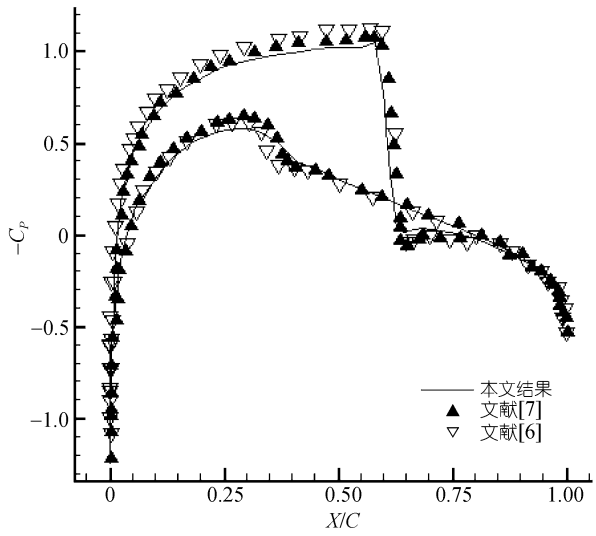

图 11 NACA 0012 翼型表面压力系数分布图(M_∞=0.8, α=1.25°)

α=0°. 台阶高 0.2, 宽 2.5, 离入口 0.5, 入口处高 1. 来流参数为 u=1, v=0, p=0.079. 此算例流动情况比较复

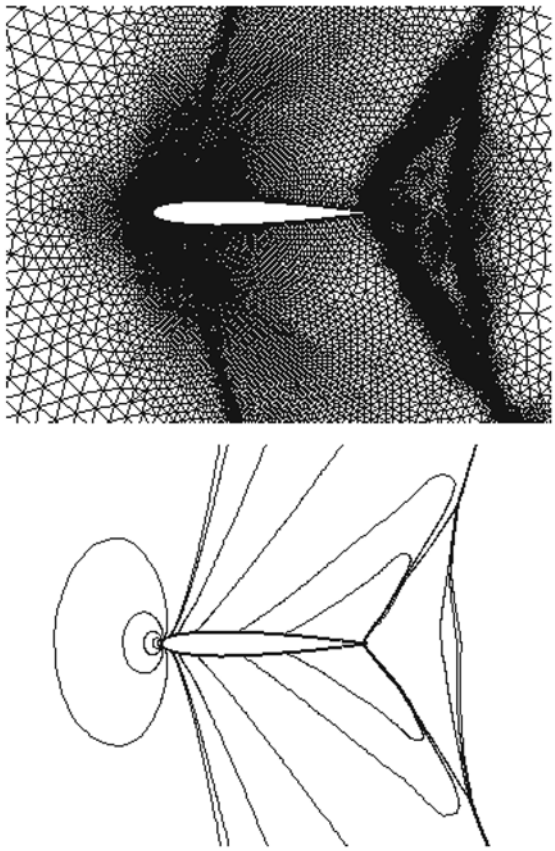

图 12　NACA 0012 翼型定常跨音速绕流自适应网格和等压线分布图(M_∞= 0.95, α = 0.0°)

NE = 113440, *NP* = 56886

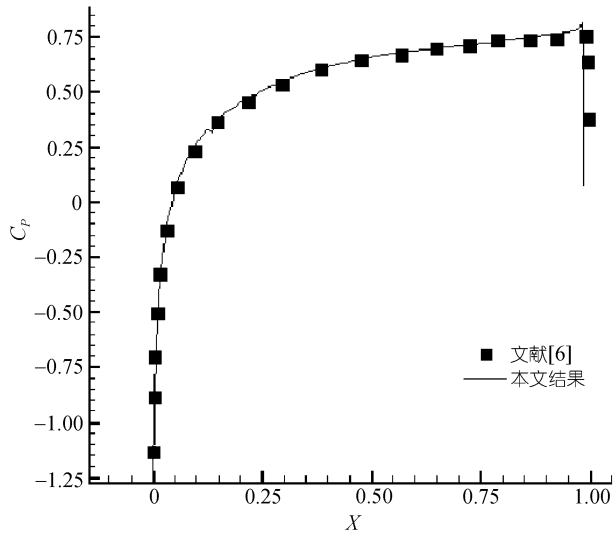

图 13　NACA 0012 翼型表面压力系数分布图(M_∞= 0.95, α = 0.0°)

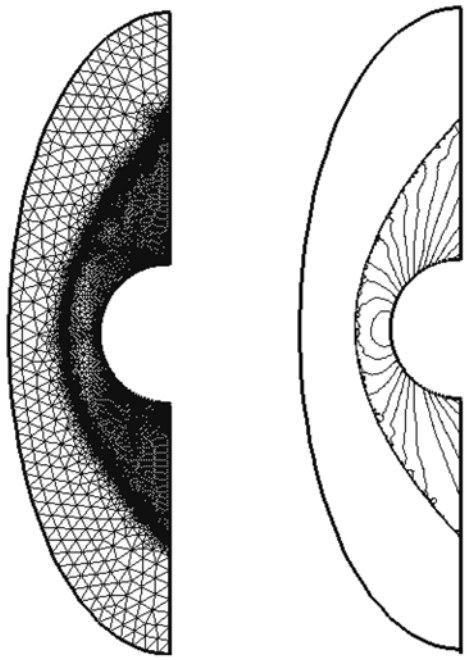

图 14　圆柱超音速绕流自适应网格和等压线分布图(M_∞= 4.0, α = 0.0°)

NE = 115739, *NP* = 58099

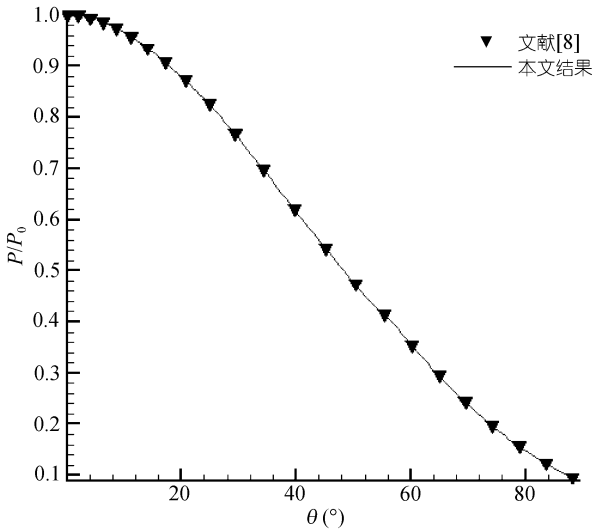

图 15　圆柱超音速绕流表面压力系数分布图(M_∞= 4.0, α = 0.0°)

杂，流场中包含激波，膨胀波和接触间断等复杂图像. 图 18 是自适应网格及等压线分布图. 算例 10 是球头超音速绕流问题，M_∞ = 7.0，这是一个轴对问题. 为验证三维算法，本算例将之当作三维问题进行计算.

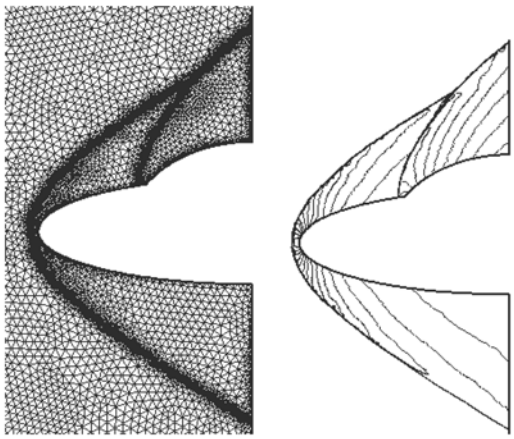

图 16 双椭圆外形的自适应网格和等压线分布图(M_∞= 4.0, α = 0.0°)

NE = 102945, *NP* = 51886

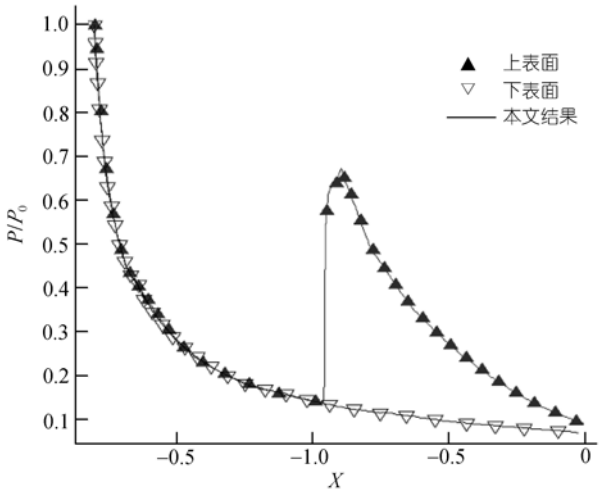

图 17 双椭圆外形表面压力系数分布图(M_∞= 4.0, α = 0.0°)

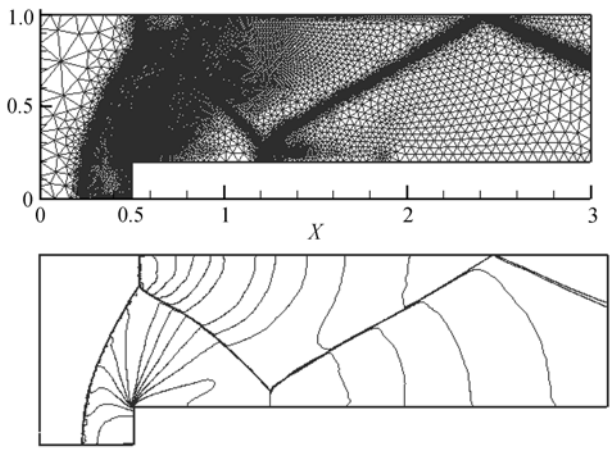

图 18 二维前台阶通道超音速流动自适应网格和等压线分布图(M_∞= 3.0, α = 0.0°)

NE = 101964, *NP* = 51242

图 19, 20 给出 *x-y* 平面上等压线分布及球面压力分布. 球面压力分布与文献[9]的结果吻合.

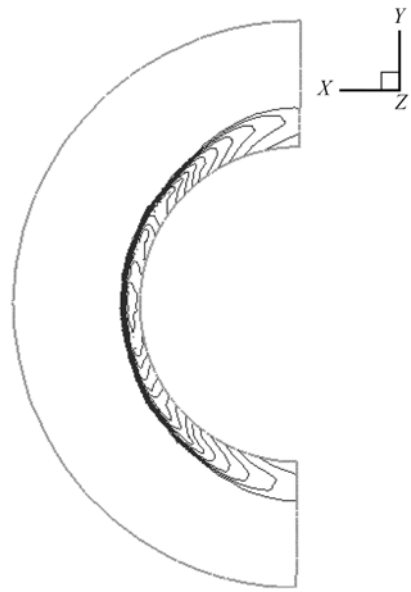

图 19 三维球头超音速绕流 *x-y* 平面上等压线分布(M_∞= 7.0)

NE = 5765669, *NP* = 905460

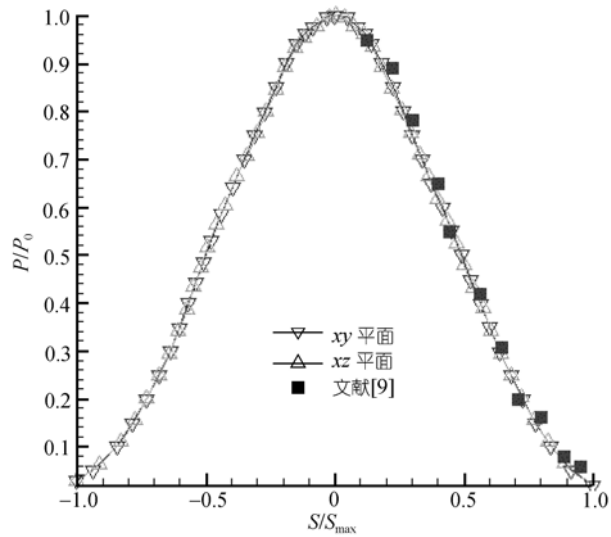

图 20 三维球头超音速绕流 *x-y* 平面和 *x-z* 平面压力沿物面的分布(M_∞= 7.0)

5 结论

(ⅰ) 本文首次提出在非结构网格上直接离散微分算子的新型数值计算方法——基函数法. 该方法是以基函数展开来逼近真实函数的. 在此基础上, 成功

地构造出在非结构网格上导数的中心格式和迎风格式. 为消除激波附近的非物理波动, 本文采用了通量分裂法及基于物理考虑的中心格式与迎风格式相结合的技术, 构造出了处理无黏可压缩流动的一阶多项式基函数格式. 一、二、三维多种典型算例表明, 此方法对间断具有高的分辨率. 采用自适应技术后, 可以得到无波动的, 精度及分辨率都十分令人满意的结果.

(ii) 基函数法成功地保留了有限差分法和有限元法的一些优点. 首先, 由于基函数法和有限元法一样是在非结构网格上构造的, 因此它能方便地处理复杂边界, 保持边界点与内点格式精度的一致, 并便于采用自适应技术改进计算的精度; 其次, 基函数法和有限差分法一样直接离散微分算子, 因而显著节约了计算时间和内存; 最后, 基函数法格式构造统一、规范, 逻辑简单, 便于编制通用程序.

(iii) 本文着重研究了一阶精度多项式类型的基函数格式. 因为与高阶精度的基函数格式相比, 一阶精度基函数格式, 公式最简单, 涉及的单元节点个数最少, 从而显著节省了计算时间和内存. 至于结果的精度和激波的分辨率则可以通过进一步加密网格来加以提高. 实践表明, 本文采用一阶多项式基函数法与自适应技术相结合的方法, 不仅显著地节约了计算时间和内存, 并且取得了精度及分辨率都很好的结果.

(iv) 本文根据物理考虑首次提出新的构造激波附近无波动格式的普适性准则.

(v) 本文对基函数法进行了初步探索, 今后还应对方法的理论基础如精度分析和稳定性分析进行研究, 此外还应对流体力学中各类微分方程和不同基函数进一步对方法进行深入数值研究.

致谢 算例 10 由沈芳博士提供, 在此致谢.

参考文献

1 张涵信. 无波动、无自由参数的耗散差分格式. 空气动力学学报, 1988, 6(2): 143—165
2 吴望一, 蔡庆东. 非结构网格上一种新型的高分辨率高精度无波动的有限元格式. 中国科学 A 辑: 数学 物理学 天文学, 1998, 28(7): 633—643
3 Peraire J, Vahdati M, Morgan K, et al. Adaptive remeshing for compressible flow computations. J Comput Phys, 1987, 72(2): 449—466[DOI]
4 谢文俊. 基函数法在三维无黏可压缩流动中的研究与应用以及三维非结构网格的生成及自适应技术研究. 硕士学位论文. 北京: 北京大学, 2002. 1—48
5 Zeeuw D D, Powell K G. An adaptively refined cartesian mesh solver for the Euler equations. J Comput Phys, 1993, 104(1): 56—68[DOI]
6 Yee H C, Harten A. Implicit TVD scheme for hyperbolic conservation laws in curvilinear coordinates. AIAA J, 1987, 25(2): 266—274[DOI]
7 Hwang C J, Wu S J. Adaptive finite upwind approach on mixed quadrilateral-triangular meshes. AIAA J, 1993, 31(1): 61—67[DOI]
8 Lyubimov A N, Rusanov V V. Gas flow past blunt bodies. NASA-TT-F715, 1973
9 Yamamoto Y. Numerical Simulation of Hypersonic Viscous Flow for the Design of H-Orbiting Plane (HOPE). AIAA Paper, 1990, 90-0601